Received: 10 February 2021 | Revised: 29 July 2021 | Accepted: 25 August 2021

DOI: 10.1111/aor.14056

Artificial Organs WILEY

MAIN TEXT

Video-based valve motion combined with computational fluid dynamics gives stable and accurate simulations of blood flow in the Realheart total artificial heart

Nathaniel S. Kelly[1] | Danny McCree[1] | Libera Fresiello[2] | Nils Brynedal Ignell[3] | Andrew N. Cookson[1] | Azad Najar[3] | Ina Laura Perkins[3] | Katharine H. Fraser[1]

[1]Department of Mechanical Engineering, University of Bath, Bath, UK

[2]Department of Cardiovascular Sciences, Katholieke Universiteit (KU) Leuven, Leuven, Belgium

[3]Scandinavian Real Heart AB, Västerås, Sweden

Correspondence
Katharine H. Fraser, Department of Mechanical Engineering, University of Bath, Bath BA2 7AY, UK.
Email: k.h.fraser@bath.ac.uk

Funding information
Engineering and Physical Sciences Research Council, Grant/Award Number: 1944013; Scandinavian Real Heart

Abstract

Background: Patients with end-stage, biventricular heart failure, and for whom heart transplantation is not an option, may be given a Total Artificial Heart (TAH). The Realheart® is a novel TAH which pumps blood by mimicking the native heart with translation of an atrioventricular plane. The aim of this work was to create a strategy for using Computational Fluid Dynamics (CFD) to simulate haemodynamics in the Realheart®, including motion of the atrioventricular plane and valves.

Methods: The accuracies of four different computational methods for simulating fluid-structure interaction of the prosthetic valves were assessed by comparison of chamber pressures and flow rates with experimental measurements. The four strategies were: prescribed motion of valves opening and closing at the atrioventricular plane extrema; simulation of fluid-structure interaction of both valves; prescribed motion of the mitral valve with simulation of fluid-structure interaction of the aortic valve; motion of both valves prescribed from video analysis of experiments.

Results: The most accurate strategy (error in ventricular pressure of 6%, error in flow rate of 5%) used video-prescribed motion. With the Realheart operating at 80 bpm, the power consumption was 1.03 W, maximum shear stress was 15 Pa, and washout of the ventricle chamber after 4 cycles was 87%.

Conclusions: This study, the first CFD analysis of this novel TAH, demonstrates that good agreement between computational and experimental data can be achieved. This method will therefore enable future optimisation of the geometry and motion of the Realheart®.

KEYWORDS

computational fluid dynamics, fluid, hemodynamics, structure interaction, total artificial heart

1 | INTRODUCTION

Worldwide 40 million people suffer from heart failure[1]; in the United States, there are 6.2 million adults with the disease.[2] Despite optimal medical treatment, some patients still do not improve, and the available therapies fail to control their symptoms. These patients need a new heart and cardiac transplantation is the gold standard treatment for these cases. However, the number of transplants is limited by the number of heart donors, and the number of donations does not meet the requirements. Hence, the number of patients listed for heart transplant continues to grow: in the United Kingdom, in the last decade, the number of patients active on the heart transplant list has increased by 134%,[3] and the situation is mirrored around the world. For patients with end-stage biventricular failure, total artificial hearts (TAHs) are a viable alternative to heart transplant.[4]

Although there are several TAHs under development, including rotary pumps, Bivacor[5] and CFTAH[6]; a positive displacement pump Reinheart[7]; and biohybrid pump, CARMAT,[8] there is only one TAH approved for clinical use, Syncardia.[9] Despite its success, the Syncardia TAH suffers from limitations including a large air compressor to move with the patient; large, transcutaneous, compressed air tubes that increase the risk of infection; and thromboembolic and hemorrhagic events.[10]

Aiming to overcome these limitations, the Realheart TAH uses the novel concept of a moving atrioventricular plane to pump blood.[11] This mechanism mimics the native human heart, in which the displacement of the atrioventricular plane accounts for 60% of the left ventricular stroke volume.[12] The Realheart consists of two pumps, each operating at the same frequency, but with the displacement of their atrioventricular planes adjusted independently to vary the stroke volume, and so achieve left–right balance. Acute tests in pigs showed the Realheart produced physiological flow and pressure waves, complete with dicrotic notch,[13,14] and virtual implantation and cadaver studies showed that a good anatomical fit would be achieved in humans.[15]

Computational fluid dynamics (CFD) has been used extensively for studying flow in rotary ventricular-assist devices[16,17] as well as rotary TAHs, including the CFTAH.[18] There are fewer uses of CFD for positive displacement TAHs: Slepian et al[9] used CFD to simulate blood flow in the Syncardia TAH and, thus, calculate the probability density function for stress accumulation, which they found differed with valve orientation; in contrast, Sonntag et al[19,20] showed that valve orientation had only a slight influence on washout in the ReinHeart TAH; and in the Carmat TAH, Luraghi et al[21] used CFD to show washout in the left heart was superior to that in the right heart. There are several issues that make modelling positive displacement pumps more challenging than rotary pumps. These include the large differences in geometry and pumping mechanisms between devices, and the presence of fluid structure interaction (FSI).

As part of the iterative design improvement process, involving in silico, in vitro, and in vivo testing, the aim of this work was to create a numerical model of the left side of the Realheart TAH and use it to investigate hemodynamics within the two chambers. The valves are important components of this TAH, and a major aspect of this work was to implement a method for modelling them. To this end, four different methods were tested. The computed pressures in the two chambers, and the flow rate produced, were compared with experimental measurements. The best method was then used to investigate the hemodynamics within the chambers including the fluid power, blood shear stresses, and washout times. Through this work, a method for studying the piston motion has been found. This will allow studies of different piston motion parameters, including stroke length, frequency, ratio of systole to diastole, and cyclic speed variation, to maximize washout, while minimizing power consumption and maintaining the low shear stresses.

2 | METHODS

2.1 | Governing equations

The governing Navier–Stokes (NS) equations were discretized using the finite-element method and solved using Autodesk CFD 2019.[22] The finite-element method has been used by other researchers for investigating blood pumps (for example[17,23]). A single Reynolds number (Re) for the whole device cannot be defined; therefore, we looked at the inlet and outlet,[24] which are pipes for which transition to turbulence has been studied, with the understanding that the geometrical features may trigger turbulence at lower Re. The maximum instantaneous Re was 4300 at the inlet, and the cycle-average Re was 1500. Studies of flow in pipes[25-27] show that during the acceleration phase the flow remains laminar for Re larger than would normally cause transition but becomes "disturbed" during the deceleration phase when there is production of turbulent kinetic energy (TKE).[26] Only if the cycle-average Re is greater than 2700 will the flow become fully turbulent.[25] Maximum Re in the ventricle chamber, based on a flow rate given by motion of the atrioventricular plane piston, was 1740. Two-equation turbulence models, such as the SST k-ω model, sometimes chosen for artificial hearts,[19,28] are parameterized for fully turbulent flows and so are not necessarily better than a laminar assumption[16] which is chosen by other authors.[21,29,30] This can be seen

in the results from the FDA CFD Benchmark medical device study,[31] in which the two-equation turbulence models gave good velocity predictions in some regions, but in other regions the laminar assumption gave better velocity predictions, and for several cases, the laminar assumption gave better pressure predictions.

As Realheart's main mechanism is the replication of the native human heart and consists of both a flexible membrane displacement and moving bileaflet valves, this becomes a fluid–structure interaction problem. The computational fluid–structure method that is used by Autodesk CFD is a masking technique, an immersed solid approach. The mesh for the solid part overlaps the fluid mesh and the fluid elements take on the instantaneous velocity of the solid. As the solid moves through the fluid, different fluid elements take the velocity of the solid part and a no-slip boundary condition at the solid surface is achieved.[32]

2.2 | Computational domain

The specific device modelled was the Realheart TAH prototype v11c (Figure 1A). Like the native heart, the fluid domain of each side of the Realheart consists of two chambers: an atrium and a ventricle. Each of these is solid on one side and has a deformable membrane at the atrioventricular plane interface (the center of the device). The two chambers are connected by a cylindrical section: within this, a prosthetic mitral valve (MV) linearly translates; and around this is a piston to compress the deformable membrane sections of the chambers. Flow enters the atrium via an inlet and passes through the cylindrical section and the open MV to the ventricle. The flow fills the ventricle as the MV moves upward in the open position. As the valve returns downward in the closed position, pressure in the ventricle is increased, and the blood is passed through the aortic valve (AV) to the outlet. Both the MV and AV are bileaflet mechanical valves.

To achieve the membrane displacement in the atrial and ventricle chambers of the computational model, a moving solid part was included. This linearly translating solid component was superimposed over the fluid chambers to reproduce the actual volumes of fluid in the chambers when in systole and diastole. Figure 1B illustrates the computational domain with fluid and solid volumes and respective boundaries.

2.3 | Mesh and discretization

The fluid and solid domains were discretized with linear tetrahedral elements, inflation layers were used to account for the high velocity gradients at the walls, and the aspect ratio was limited to 50. The MV and AV were meshed as surfaces, as opposed to volumes, to reduce computational time. A mesh study was performed on four mesh densities: coarse, medium, fine, and very fine. The total number of elements of both solid and fluid domains is given in Table 1, and increases by an order of magnitude in line with CFD "Best Practices".[31]

The modified Petrov–Galerkin upwind method for the advection terms in the momentum equation was used as part of spatial discretization. Transient discretization was achieved using the backward difference method, which is an implicit discretization scheme requiring iterative solution within each timestep.[33] A timestep of 0.005 seconds was used.

2.4 | Rheology and boundary conditions

Blood was assumed to be shear-thinning with Carreau rheology (Equation 1) and effective viscosity, μ.[34] The constants were as follows: high shear rate viscosity μ_∞ = 0.0035 Pa.s, zero shear viscosity $\mu_0 = 0.056$ Pa.s, relaxation time constant $\lambda = 3.313$ seconds, and power-law index n = 0.356.

$$\mu = \mu_\infty + (\mu_0 - \mu_\infty)[1+(\lambda\gamma)^2]^{\frac{(n-1)}{2}} \quad (1)$$

Pressure boundary conditions were prescribed at the inlet and outlet (P_{in} = 15 mm Hg, P_{out} = 70 mm Hg) of the flow domain. Inlet pressure was an approximate value for pulmonary venous pressure estimated from the pulmonary artery and left atrial pressure measurements obtained from in vivo testing of the Realheart[14] and estimating pulmonary venous pressure from those.[35] The outlet pressure was an approximate value for mean pressure in the small arteries, where the pressure pulse has a reduced magnitude, and the value was obtained using systolic and diastolic aortic pressure from,[14] estimating pressure in the small arteries according to[36] and then assuming mean arterial pressure = 2/3 diastolic pressure + 1/3 systolic pressure. Inspired by Coccarelli et al,[37] to simulate the resistance of the aorta and large arteries, a porous media component was included in the fluid domain upstream of the outlet. This allowed flow in the aorta to develop natural pulsatility without prescribing the time-varying pressure. For steady flow of a Newtonian fluid the pressure drop ΔP across a porous medium is described by Darcy's law (Equation 2).

$$\Delta P = -\frac{\mu}{\kappa} VL \quad (2)$$

Here the permeability constant is κ, viscosity, μ, bulk velocity, V, and length over which the resistance acts, L. Following a method similar to that used by Sonntag et al,[19] the permeability constant, κ, for the porous media component in the

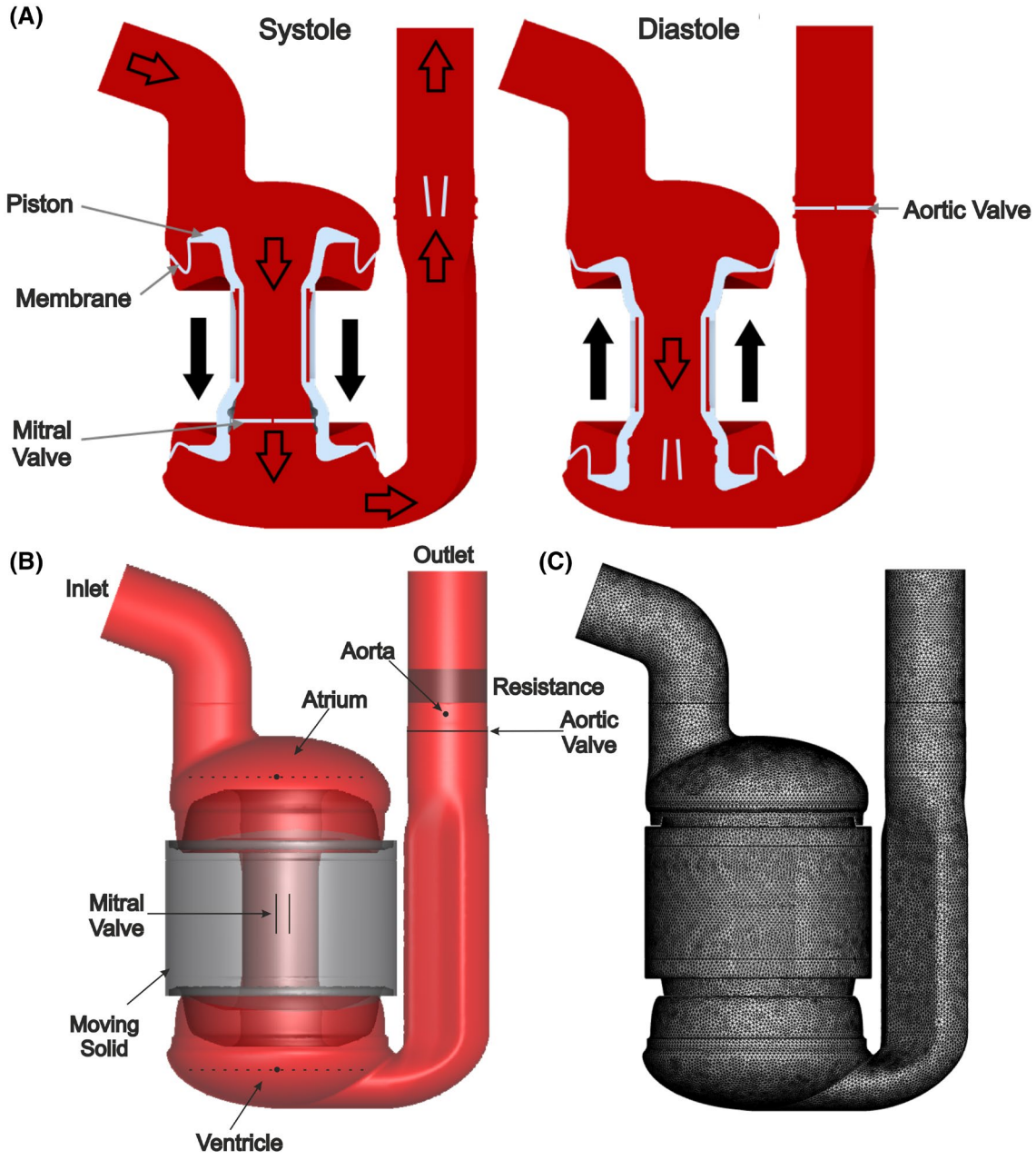

FIGURE 1 A, Schematic diagram showing the working principle of the Realheart: during systole the mitral valve is closed and the piston moves down pushing blood out through the aortic valve; during systole the piston moves up, the mitral valve opens and the aortic valve closes allowing the ventricle to refill with blood. B, Computational domain used for CFD analysis. Gray components indicate solid domain, red parts indicate fluid domain, dark red indicates the porous resistance section. Dotted lines indicate the positions where velocity profiles were obtained and larger dots mark locations where the pressure was monitored. C, The mesh used for the study [Color figure can be viewed at wileyonlinelibrary.com]

fluid domain, was adjusted in repeated simulations to give a pulse pressure of approximately 50 mm Hg, which resulted in $\kappa = 0.0148$ mm^2 with $L = 10$ mm.

2.5 | Plane and valve motion strategies

The Realheart device consists of three moving components: membrane displacement, translating and rotating MV leaflets, and rotating AV leaflets. The motion of the piston was sinusoidal and controls the atrioventricular plane including the MV, with a specific amplitude, or half the stroke length $A = 12.5$ mm, a total time for the downward motion, the systolic phase T_{systole}, and a total time for the upward motion, the diastolic phase T_{diastole}. These times are variable and currently set according to Equations (3) and (4) [38]:

$$T = T_{\text{systole}} + T_{\text{diastole}} \tag{3}$$

$$T_{\text{systole}} = (541 - 132/T)/1000 \tag{4}$$

The motion of the atrioventricular plane, which drives the pump, was then specified according to Equation (5):

$$x = \begin{cases} A\cos\left(\omega_{\text{systole}} t\right) - A, 0 < t \le T_{\text{systole}} \\ A\cos\left(\omega_{\text{diastole}}\left(t - T_{\text{shift}}\right)\right) - A, T_{\text{systole}} < t \le T, T_{\text{shift}} = T_{\text{systole}} - T_{\text{diastole}} \end{cases} \tag{5}$$

Here, ω is the angular frequency ($\omega_{\text{systole}} = \pi/T_{\text{systole}}$ and $\omega_{\text{diastole}} = \pi/T_{\text{diastole}}$) and t is time. The motion of the plane is shown in Figure 2: it begins at the origin (top) at the start of systole and moves downward. In this study the heart rate was 80 bpm so $T = 0.75$ seconds.

One aim of this work was to assess four different strategies for implementing the opening and closing rotational motions of the valve leaflets to find the most accurate method. These four strategies were (1) assumed perfect opening and closing of the valves, (2) flow-driven opening and closing, (3) MV opening and closing angles obtained from experiments and AV flow-driven, and (4) MV and AV opening and closing angles from experiments. The four strategies are described in detail below.

1. The MV closed at the maximum vertical plane displacement during diastole and opened at the minimum displacement during systole. The AV motion was synchronized to the MV so that it opened as the MV closed and closed as the MV opened. The time taken for either valve to open or close was one numerical timestep (Figure 2A).
2. The opening and closing of both MV and AV are determined by the fluid torques exerted on the valves. This is the most realistic flow configuration that was applied. The changes in pressure, and flow through the valves, should cause the leaflets to open and close at the correct time. In Autodesk CFD, flow-driven motion was implemented by enabling the "*flow-driven*" option in the motion setup and applying maximum and minimum bounds for rotation angles of the valve leaflets.
3. MV motion from experiments (see 4) and AV flow-driven (see 2).
4. Experiments were performed with the Realheart in a water test rig operating at heart rates 60-120 bpm, and videos showing the valve motion were recorded. Videos had a frame rate 200 Hz and were analyzed using the Image Processing Toolbox in MATLAB (Release

TABLE 1 Mesh densities for the four meshes used in the mesh study

	Mesh density	No. of solid elements	No. of fluid elements	Total no. of elements
1	Coarse	293 034	396 391	689 425
2	Medium	1 098 448	1 473 319	2 219 873
3	Fine	1 192 196	1 636 010	2 828 206
4	Very Fine	2 129 461	2 929 543	5 059 004

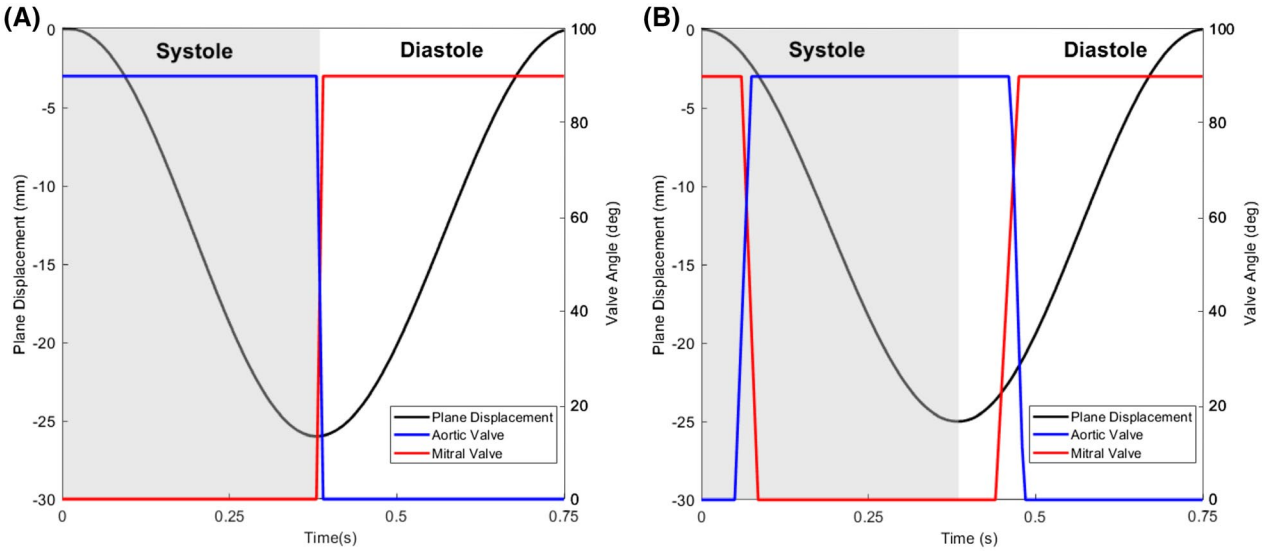

FIGURE 2 A, Atrioventricular plane motion used for strategy (1), (2) and (3), and valve angle motion for strategy (1). B, Atrioventricular plane and valve angle motion used for strategy (4). The plane displacement uses the left-hand vertical axis, whereas the valve angles are shown by the right-hand vertical axis [Color figure can be viewed at wileyonlinelibrary.com]

2016b, The MathWorks, Inc, Natick, Massachusetts, United States) where the motion of the atrioventricular plane, and the angular rotation of the MV and AV were extracted. The experimental motion of the atrioventricular plane was then used to synchronize the experimental valve leaflet opening and closing times with the theoretical sinusoidal atrioventricular plane motion, to produce the input data on the valve motions for the CFD simulations (Figure 2B).

2.6 | Simulation postprocessing

To evaluate the efficiency of the Realheart, the fluid power consumption of the device was computed. This was estimated by calculating the hydraulic force exerted on the fluid, from the moving components.

Shear stresses were examined by thresholding at different values, 10 and 15 Pa, and manually searching through the timesteps to find when these stresses occurred. These threshold values were not meant to represent any specific type of blood damage but were indicative of the shear stresses present.[39] In general, blood damage is a function of both shear stress magnitude and exposure time, and therefore a model incorporating both would be required to predict actual blood damage.[40]

Washout was assessed by solving an advection–diffusion equation for an additional scalar representing new blood. The concentration of the additional scalar was 0 at time 0, and at the inlet boundary the concentration was 1 at all timesteps. The scalar then showed how long it took for the old blood to be washed out of the Realheart to be replaced with new blood, while the spatial variation revealed the regions in which the old blood persisted. Following Luraghi[21] the washout was simulated for four cycles.

2.7 | Hybrid rig experiments

A hybrid cardiovascular simulator was adapted to test and characterize the hemodynamic behavior of the Realheart TAH, and the study was previously reported.[41] Briefly, the hybrid simulator was comprised of a computational and a hydraulic component: the computational domain was a lumped parameter model of the cardiovascular system; the hydraulic domain included four "hybrid interfaces" where the TAH was connected to interact with the rest of the circulation. Pressure sensors (PPG Honeywell, Columbus, OH, USA) measured the pressure in the hydraulic chambers mimicking the aorta and the left atrium. Additionally, a TruWave pressure transducer (Edwards Lifesciences, Irvine, CA, USA) was used to measure the pressure in the left artificial ventricle of the Realheart TAH. Flow rates were measured using Transonic flowmeters (ME 24 PXN, T402 Transonic Systems Inc, Ithaca, NY) placed at the outlet of each artificial ventricle.

3 | RESULTS

3.1 | Mesh study

Mesh quality was assessed using the aspect ratio, which varied between 1 and 48.5 with a mean value 1.7. Mesh sensitivity was evaluated by comparing the pressure and velocity fields with the four different meshes. The fine and very fine meshes captured changes in pressure through time, and were very similar, compared with the coarse and medium meshes (Figure 3A). The cycle-averaged, absolute difference in pressures between fine and very fine meshes was 4.09 mm Hg, which was 2.1% of the peak pressure. Measurements of velocity along the cross section in the ventricle at mid-diastole were obtained (the line indicated in Figure 1B). The velocity profiles were smoother for the fine and very fine, compared with the more irregular shape for the coarse and medium meshes (Figure 3B). The average absolute velocity difference between fine and very fine was 0.0156 m/s, which was 2.8% of the maximum. The fine mesh was deemed adequate to simulate both pressure and velocity fields and was used for the remaining simulations providing a balance of accuracy and computational time.

3.2 | Pressure and flow

Simulated pressures in the atrium, ventricle, and aorta were compared between each of the four motion simulation strategies (Figure 4). The simulated pressure in the ventricle was compared with that measured in the hybrid rig experiments[41] (Figure 4). The cycle mean values for the pressures were also compared (Table 2).

The results showed that when using strategy (2), there was significant numerical instability (Figure 4) and the general pressure waveforms for each chamber were nonphysiological. This was also the case for strategy (3), in which the AV was flow-driven, and large spikes in ventricular pressure were seen (Figure 4). Ventricular pressure measurements were the most sensitive parameter for each of the strategies. The mean ventricular pressure calculations for strategies (1) and (4) both showed good agreement with experimental measurements (Table 2). Comparing waveforms of (1) and (4) (Figure 4), negative and positive spikes in pressure were

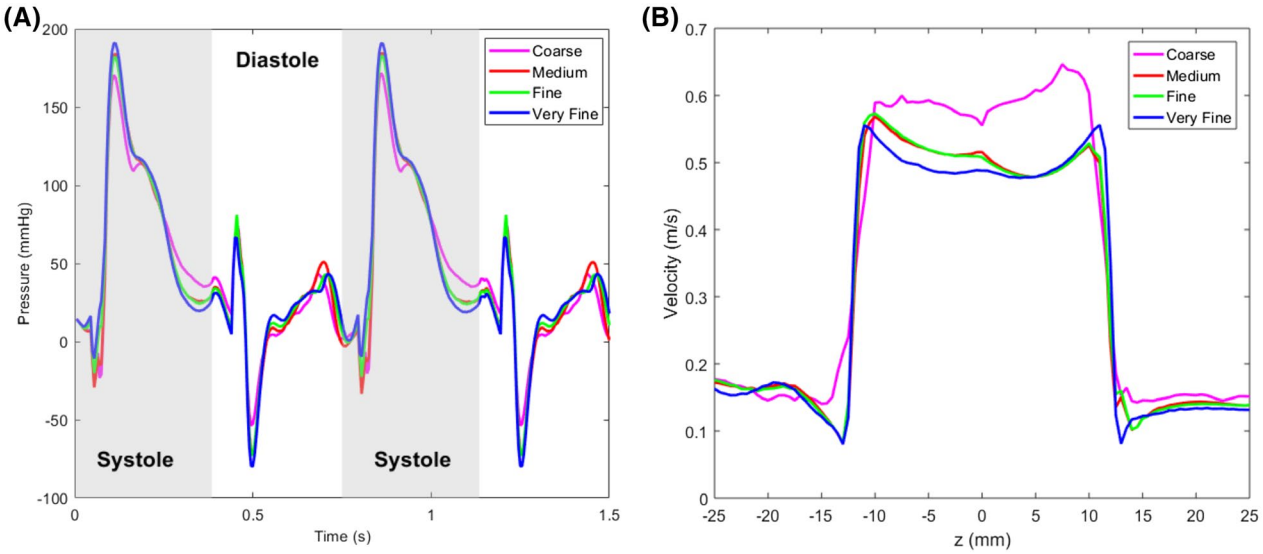

FIGURE 3 Mesh sensitivity (A) comparison of ventricle pressure on different meshes, at the location shown in Figure 1, throughout time (B) comparison of velocity profiles during mid-diastole on a line through the ventricle, as shown in Figure 1 [Color figure can be viewed at wileyonlinelibrary.com]

observed, at times corresponding to the valves opening and closing; however, strategy (1) showed small perturbations of instability before these increases in pressure. The waveform for strategy (4) had the best qualitative agreement with the experiment.

Velocity fields for strategies (1) and (4) are given in Figure 5 at mid-diastole. The velocity fields were very similar; however, using strategy (1), there were regions of higher velocity downstream of the MV, in addition to the areas of lower flow from the ventricle to the AV. In both strategies (1) and (4) as the MV opened two counter-rotating vortices formed between the valve leaflets (seen by the slow flow regions in Figure 5), effectively blocking that portion of the MV orifice.

A mean flowrate of 4.24 L/min was found when using strategy (4), showing good agreement with the experimental data (Table 2). In contrast, strategy (1) predicted a much higher flow rate of 5.19 L/min. Variation in flow rate through time at the inlet and outlet were compared between these two strategies (Figure 6). Peak flow rate was larger with strategy (1) than strategy (4). Both strategies predicted some reverse flow at either the inlet and/or the outlet. Reverse flow at the outlet is due to imperfect closing of the AV, and so is larger with the video-based motion of strategy (4) because strategy (1) has perfect valve motion and so prohibits regurgitant flow. Reverse flow at the inlet was larger with strategy (1), which is related to the earlier closure of the MV.

The results of the motion study show that the flow-driven motion implemented for the valves is prone to numerical instability. Using the motion taken from videos provides more realistic behavior of the device, so strategy (4) was used in the remaining analysis to calculate power consumption, shear stress, and washout.

3.3 | Hydraulic power and efficiency

There was a large peak in the power consumption during systole, and a second, smaller peak in the power consumption during diastole (Figure 7). The main peak was due to the work required to push the fluid out of the ventricle against the arterial pressure, and the second peak was the work required to push the blood from the atrium through to the ventricle. The mean, cycle-averaged fluid power consumption was 1.03 W. The fluid power efficiency was then calculated as the ratio of mean power out (outlet flow rate multiplied by aortic pressure) to power consumption and found to be 0.82.

3.4 | Shear stress

The largest shear stresses occurred during diastole as the atrioventricular plane moved upward and blood flowed through the MV to fill the ventricle. Shear stresses at the 10 Pa threshold lasted for approximately 200 ms while shear stress regions at the 15 Pa threshold were smaller and their duration was reduced to 125 ms (Figure 8). The largest regions occur along the wall around the MV over a length of around 25 mm. Toward the atrium two smaller regions of stress occur as the diameter changes: The isovolumes were approximately 4 mm in size at 15 Pa, at 10 Pa they were double the size with varying shape and morphology. No shear stresses at these thresholds were found around the AV.

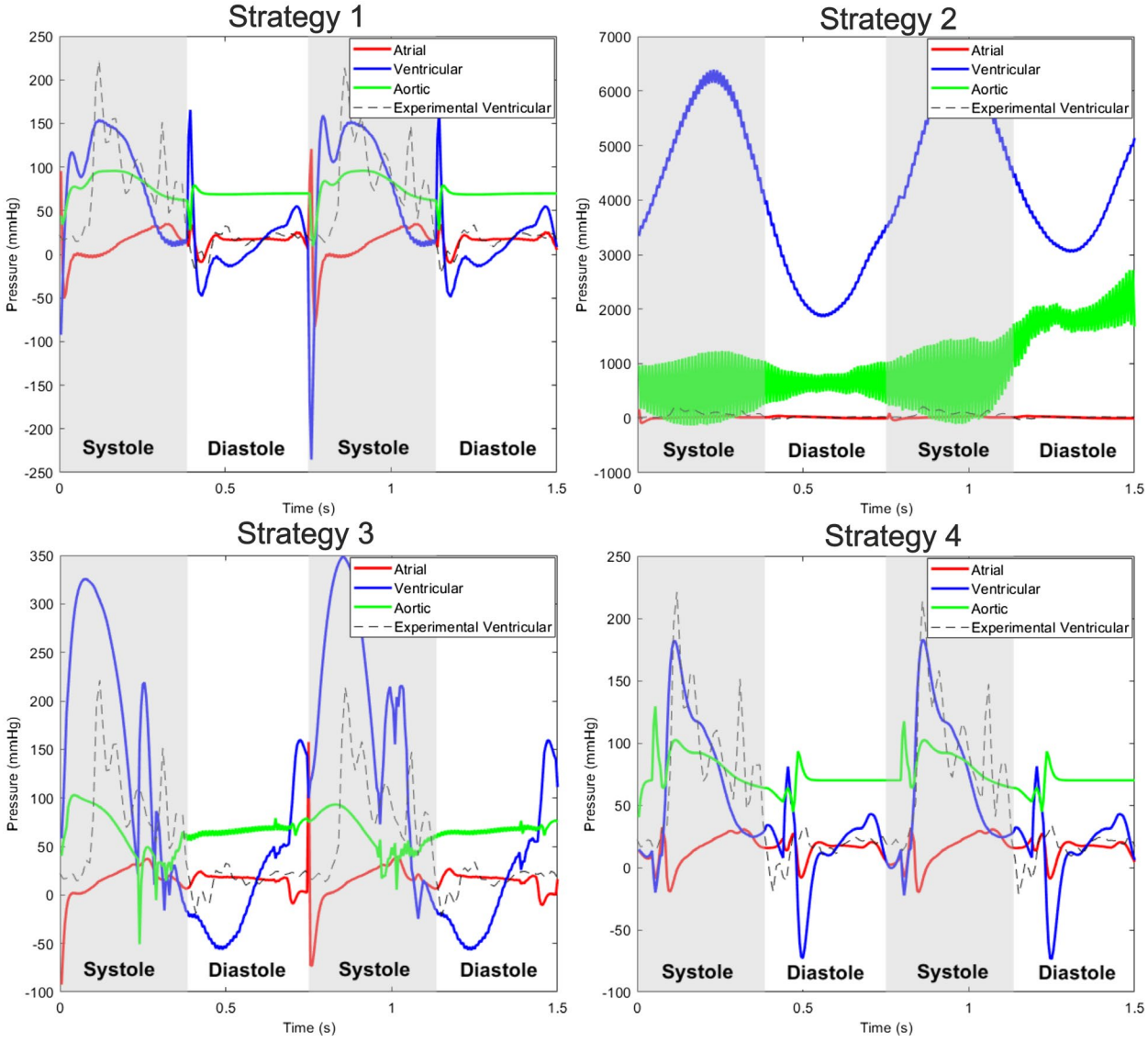

FIGURE 4 Simulated pressure waves in the atrium, ventricle, and aorta, at the locations shown in Figure 1, for the different valve motion strategies, compared with experimental pressure in the ventricle [Color figure can be viewed at wileyonlinelibrary.com]

TABLE 2 Pressures in the ventricle, atrium, and downstream aortic valve for each strategy, compared with experiments

Strategy	Mean ventricular pressure (mm Hg)	Mean atrial pressure (mm Hg)	Mean aortic pressure (mm Hg)	Outlet flowrate (L/min)
1	48.15	15.1	74.1	5.19
2	3454.4	14.8	580.7	–
3	95.7	14.3	64.6	–
4	43.2	15.1	74.8	4.24
Experimental	45.7	7.4	84.5	4.46

3.5 | Washout

After the four cycles the concentration of new blood in the ventricle was 87% and at the AV was 84% (Figure 9). The concentration increase appears to oscillate around an exponential, which agrees with a similar type of washout study on rotary VADs,[42] so the remaining 16% will take longer to wash out than the first 16%. The regions that

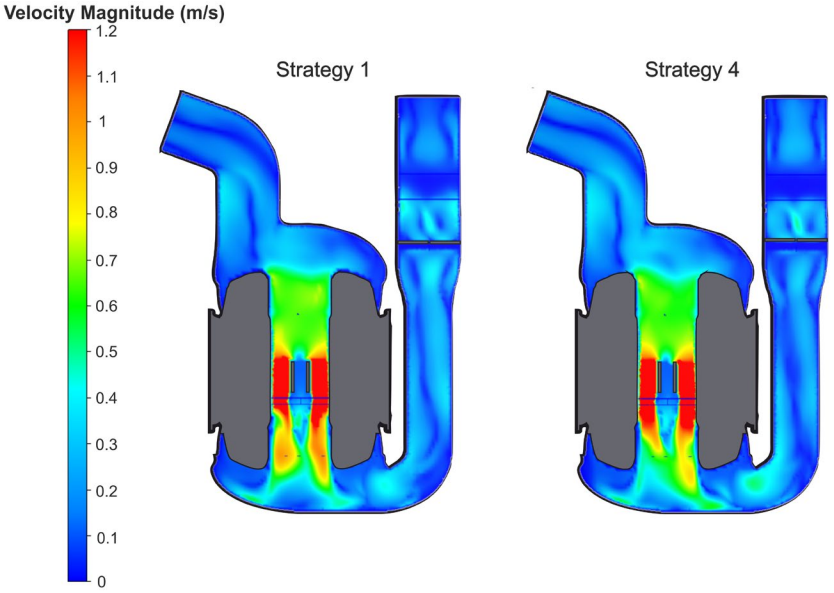

FIGURE 5 Comparison of velocity fields at time 0.6 seconds (mid diastole) for strategy (1) and strategy (4) [Color figure can be viewed at wileyonlinelibrary.com]

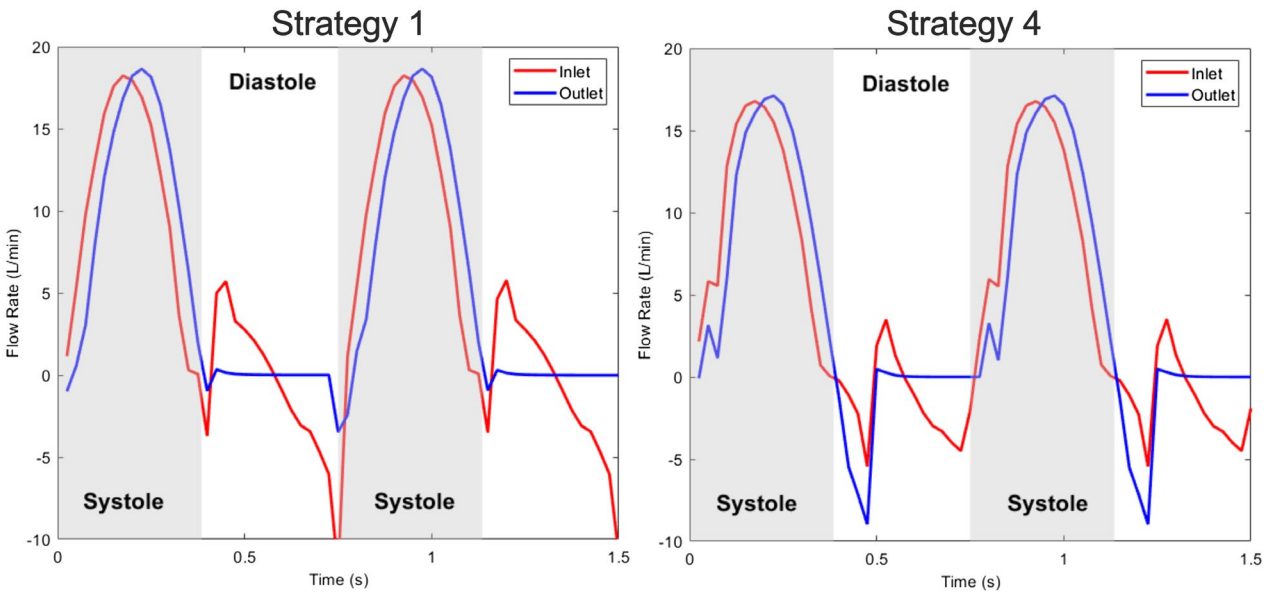

FIGURE 6 Temporal variation in inlet and outlet flowrate for strategy (1) and strategy (4) [Color figure can be viewed at wileyonlinelibrary.com]

took longest to washout were located around the edges of the membranes in both the atrial and ventricle chambers, and along the inner side of the outlet "chimney" section. Because there are no regions with a concentration of new blood equal to 0 at the end of the four cycles, all regions are washing out and there are no stagnation regions.

4 | DISCUSSION

The Realheart TAH is a complex device, consisting of several moving parts: through a combination of the semisinusoidal movement of the atrioventricular plane and MV, consequent opening and closing of the MV leaflets, and subsequent closing and opening of the downstream AV, a pulsatile flow and pressure are created. The aim of this work was to overcome these simulation challenges to create a CFD framework for the Realheart TAH. To this end, four different strategies for simulating the valve motions were assessed, and the most accurate was used to analyze power consumption, shear stresses, and washout.

The prescribed motion of strategy (1) will always give a flow rate equal to the stroke volume, created by the motion of the piston in the ventricle, multiplied by the heart rate. Then strategy (1) cannot account for the potential presence of regurgitation, which could occur if the valves open and close at different times. This motion of the device gave sharp increases, or "spikes," in pressure in the

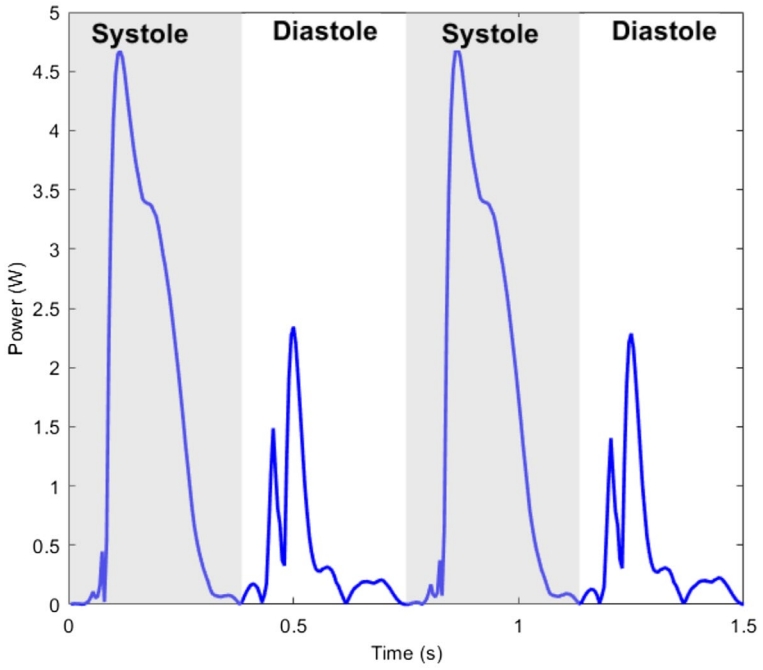

FIGURE 7 Temporal variation in power consumption with strategy (4) [Color figure can be viewed at wileyonlinelibrary.com]

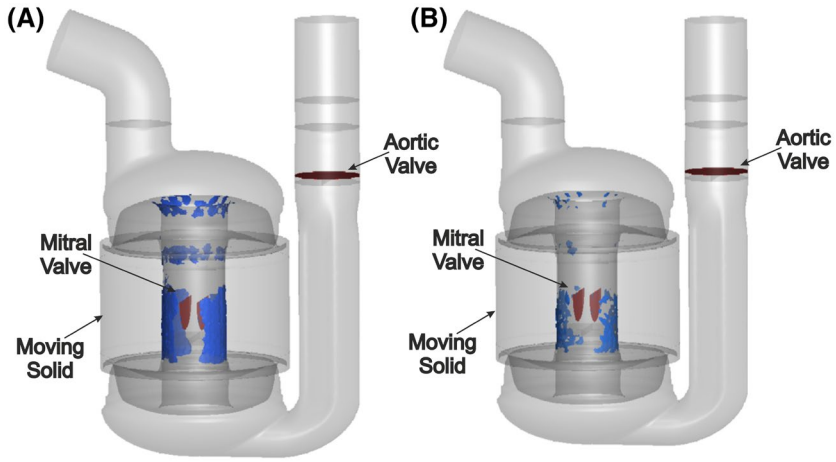

FIGURE 8 Shear stress isovolumes at thresholds of (left) 10 Pa and (right) 15 Pa during mid-diastole at $t = 0.525$ seconds [Color figure can be viewed at wileyonlinelibrary.com]

ventricular chamber. These occurred at times when both the MV leaflets and AV leaflets were changing angle and were assumed to be due to the difference between the prescribed valve motion and that which should occur. Reducing the size of the timestep increased the magnitude of the spikes, although the rest of the ventricular pressure wave remained consistent with the 0.005 seconds timestep used.

The flow-driven strategy (2) uses the torque from the fluid flow acting on the valve leaflets to open and close them, thus representing the actual mode of operation in vitro. The aim of this strategy was to be able to calculate opening and closing times of the valves at the physically correct times. While the fluid forces act on the valve leaflets to cause accelerations, the induced motion of the leaflets in turn exerts forces on the fluid, thus altering the flow. This fluid–structure interaction resulted in high numerical instability, which could likely be resolved in future by using different software, which has increased functionality, greater control of numerical method settings, and more flexible scope for user-defined interaction. Fluttering and flapping motions of the MV leaflets were observed, causing the AV not to open.

In strategy (3), a prescribed MV motion was introduced, with a flow-driven AV with the aim of overcoming the instability found with strategy (2). Although the simulated pressures were within a more realistic range, the AV still did not open and close correctly, and there were insufficient controls within Autodesk CFD to enable stable flow-driven motion.

Comparison of the velocity fields between (1) and (4) showed minimal differences, indicating that although the timing of the valve motion has a large influence on the pressure waves during the opening and closing of the

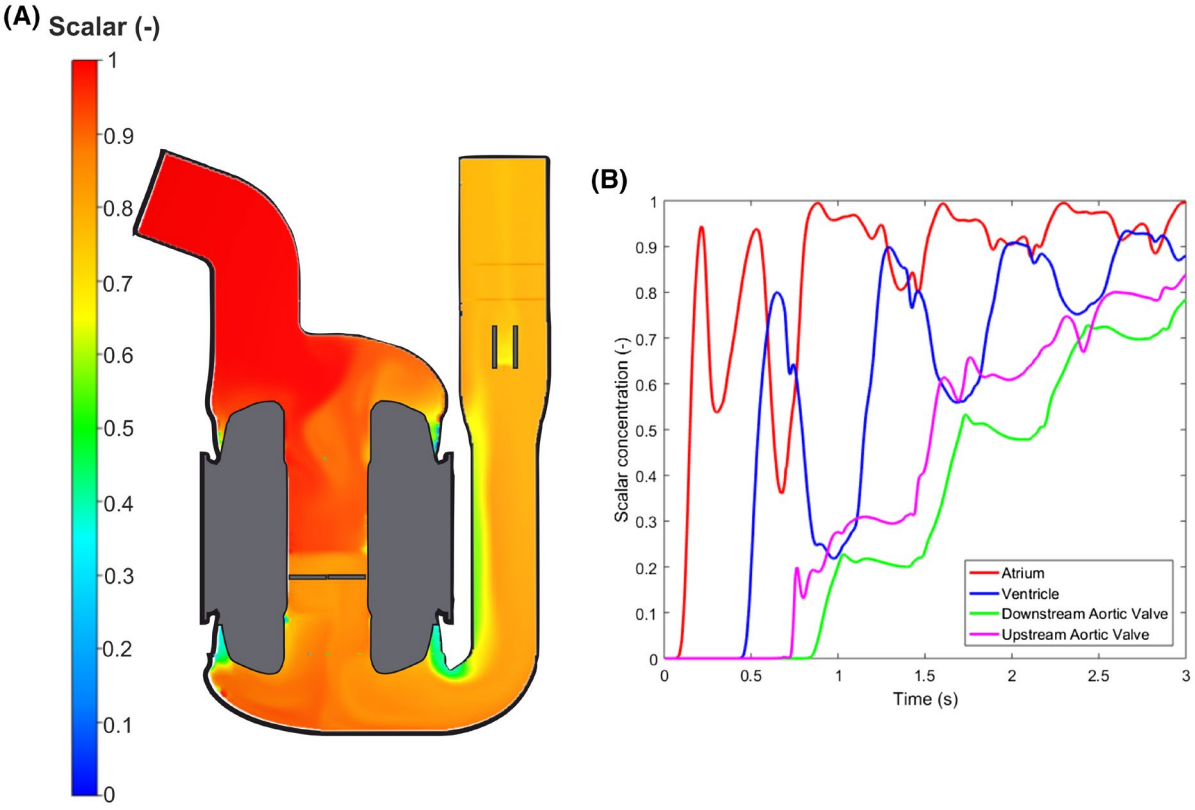

FIGURE 9 (Left) Spatial variation in concentration after four cycles and (right) temporal variation in concentration in the different regions of the device [Color figure can be viewed at wileyonlinelibrary.com]

valves, this does not have a large influence on the velocity field through the remainder of the cycle, which is more influenced by the piston motion. A cycle averaged difference of 0.26% for atrial and 10.7% for ventricular pressure was found when comparing strategies (1) and (4). Compared with experimental data, there were cycle-averaged differences of 5% and 6% in ventricular pressures from strategies (1) and (4), respectively. Comparing average flow rates, the differences between experiment and simulation were 16% and 5% for strategies (1) and (4), respectively, and, therefore, strategy (4) was selected for the remaining analysis.

The shape of the ventricular pressure wave from strategy (4) was in good qualitative agreement with the experimental measurements although the experimental values oscillate more such that the maximum pressure is larger in the experiment. These oscillations may come from reflected waves, which are not modelled in the simulation boundary conditions. The minimum ventricle pressure in the simulation has a larger negative than the experiment; this is caused by a vacuum effect occurring as the MV starts to move away from the ventricle, and before the MV has started opening, when the volume of the incompressible fluid is fixed. Small differences in timing of the valve leaflets opening or closing make a large difference in the pressures at these times, which can be seen by comparing the results for strategies (1) and (4). It is likely that the lower minimum ventricle pressures in the simulations compared with the experiments are the result of remaining small errors in the precise timing of the motion of the valve leaflets, which rely on correctly identifying the exact times at which the valves start to open and finish closing. Due to the translation of the MV, and limited viewing angle due to requiring a transparent window through which both the MV and AV could be seen simultaneously, the MV was not always in focus and so there was an error associated with identifying the exact initial opening and complete closing times. Any small timing errors are accentuated by the vacuum effect described above. The small negative pressures found experimentally in the ventricle are not expected to be a problem because even large negative pressures (600 mm Hg) do not cause blood damage, except in the presence of an air interface.[43] Small, negative pressures calculated in the atrium should be further investigated because these could result in suction on the venous system. However, these are likely to be alleviated by the new preload sensitive version of the Realheart currently under development.[41]

The flow rate from strategy (4) was in good agreement with the experimental flow rate (difference 0.22 L/min). There was reverse flow at the outlet, which occurred as the AV closed (8.53 mL) and some reverse flow at the inlet,

which occurred as the piston moved away from the ventricle, firstly just before the MV opened (3.31 mL), and then again as the piston neared its maximum displacement (7.87 mL). The reverse volume found for the AV is similar to the total regurgitant volume measured for bileaflet mechanical heart valves under aortic pressure conditions, which was 6.0 mL.[44] The impact of regurgitation on blood damage in a mechanical heart valve within the Realheart still needs to be assessed.

The average fluid power consumption from strategy (4) was just 1.03 W for the simulated left side of the Realheart. This value is a measure of the power transmitted to the fluid, and as such does not account for the losses, electrical and thermal, between the power supply and the fluid contacting moving components.

Shear stresses calculated using strategy (4) were low compared with rotary blood pumps, where similar computational studies have identified that significant regions of shear stresses greater than 150 Pa can exist[39,45,46] and were concentrated around the moving MV. Based on these results, there should not be a problem with high shear stresses. However, blood damage also depends on exposure times. To provide some indication of the potential for blood damage, a washout study was performed. This showed that after four pump cycles 13% of the original blood remained. This compares well with the Carmat, now in clinical trials,[47] which after four cycles, had 6.2% remaining in the left heart and 15% in the right heart.[21] There were small specific regions in which the blood spent longest, which were located around the membranes. Eliminating these regions, for example with minor geometrical changes, might serve to enhance the washout properties even further.

4.1 | Limitations

Because the Reynolds numbers were low, we assumed the flow was predominantly laminar and solved the NS equations to simulate the fluid flow. To assess the impact of this choice an additional simulation solving the Reynolds Averaged Navier–Stokes (RANS) equations using the SST k-ω model for turbulence was conducted using strategy 4. The resulting pressure in the ventricle was slightly different to the original NS solution with a cycle average absolute difference of 8.5 mm Hg, slightly lower mean (41.7 vs. 43.2 mm Hg) and slightly higher maximum (198 vs. 191 mm Hg). The TKE was small, generally <0.1 mJ/kg with maximal values around 1 mJ/kg for short periods, which is comparable with simulations of a fully functional bileaflet mechanical heart valve in which the maximum TKE was 1.1 mJ/kg.[48] Because the pressure differences were small, and the TKE using SST was found to be small, our choice of solving NS is justified.

The main limitations to this work are the omission of the deformable membranes and blood damage models. In the future, a full fluid–structure interaction simulation of the membranes should be incorporated to account for variations in flow and pressure due to different preloads and afterloads. Afterload also influences the opening and closing time of the AV, so to incorporate afterload changes into our simulation strategy, it will be necessary to record more valve motion videos. To fully investigate blood damage, numerical models for hemolysis (eg,[39,49,50]) and thrombosis (eg,[51]) will be included and used to optimize control of the atrioventricular plane, so as to minimize any possible damage. The simulation methods developed here will be used to assess the impact of the design changes in the new version of the Realheart in development. Other limitations include geometry simplifications, such as the valve leaflet thickness and closing angle of the valves, and the use of a porous section to mimic downstream vascular impedance but without compliance. In the future, we will use the methods developed to optimize the piston motion, including stroke length, frequency, ratio of systole to diastole, and cyclic speed variation, to maximize washout, while minimizing power consumption and maintaining the low shear stresses.

5 | CONCLUSION

With the increase in transplant waiting times the development of TAHs is vital for patients with end-stage heart failure, and simulations are a valuable tool in this process. In this work, CFD simulations of the Realheart were performed and strategies for taking account of the FSI in the mechanical valves were investigated. The work showed that in the absence of a functioning FSI solver the valve motion can be incorporated using a prescribed motion obtained from video analysis of the moving valves. There was good qualitative agreement between the calculated and measured ventricle pressures, and the error in the flow rate was 5%. The simulations showed low shear stresses with regions experiencing up to 15 Pa. Washout simulations showed 87% of blood was washed out in four pump cycles, which is comparable with other pulsatile TAHs.

ACKNOWLEDGMENTS

This study was partially funded by Scandinavian Real Heart AB. NSK has an EPSRC DTP studentship (Reference: 1944013).

DISCLOSURES

NBI, AN, and ILP are employees of or consultants to and/or shareholders of Scandinavian Real Heart AB.

AUTHOR CONTRIBUTIONS

Concept/design: Perkins, Fraser
Simulations/experiments: Kelly, McCree, Fresiello, Brynedal Ignell
Data analysis/interpretation: Kelly, Cookson, Fraser
Drafting article: Kelly, Fraser
Critical revision of article: Fresiello, Brynedal Ignell, Cookson, Najar, Perkins
Approval of article: Kelly, McCree, Fresiello, Brynedal Ignell, Cookson, Najar, Perkins, Fraser.

ORCID

Andrew N. Cookson https://orcid.org/0000-0002-5382-5116
Katharine H. Fraser https://orcid.org/0000-0002-7828-1354

REFERENCES

1. Vos T, Allen C, Arora M, Barber RM, Bhutta ZA, Brown A, et al. Global, regional, and national incidence, prevalence, and years lived with disability for 310 diseases and injuries, 1990-2015: a systematic analysis for the Global Burden of Disease Study 2015. Lancet. 2016;388(10053):1545–602. https://doi.org/10.1016/s0140-6736(16)31678-6
2. Benjamin EJ, Muntner P, Alonso A, Bittencourt MS, Callaway CW, Carson AP, et al. Heart disease and stroke statistics—2019 update: a report from the American Heart Association. Circulation. 2019;139(10):e56–28. https://doi.org/10.1161/cir.0000000000000659
3. Statistics and Clinical Studies, NHS Blood and Transplant. Organ donation and transplantation activity report 2018/19; 2019. Available from: https://nhsbtdbe.blob.core.windows.net/umbraco-assets-corp/16537/organ-donation-and-transplantation-activity-report-2018-2019.pdf
4. Cook JA, Shah KB, Quader MA, Cooke RH, Kasirajan V, Rao KK, et al. The total artificial heart. J Thorac Dis. 2015;7:2172–80.
5. Timms D, Fraser J, Hayne M, Dunning J, McNeil K, Pearcy M. The BiVACOR rotary biventricular assist device: concept and in vitro investigation. Artif Organs. 2008;32:816–9.
6. Kado Y, Byram N, Miyamoto T, Horvath DJ, Kuban BD, Sale S, et al. Continuous-flow total artificial heart: hemodynamic and pump-related changes associated with posture in a chronic calf model. J Artif Organs. 2019;22:256–9.
7. Pelletier B, Spiliopoulos S, Finocchiaro T, Graef F, Kuipers K, Laumen M, et al. System overview of the fully implantable destination therapy—ReinHeart-total artificial heart. Eur J Cardiothorac Surg. 2014;47:80–6.
8. Mohacsi P, Leprince P. The CARMAT total artificial heart. Eur J Cardiothorac Surg. 2014;46:933–4.
9. Slepian MJ, Alemu Y, Soares JS, G. Smith R, Einav S, Bluestein D. The Syncardia™ total artificial heart: in vivo, in vitro, and computational modeling studies. J Biomech. 2013;46:266–75.
10. Torregrossa G, Morshuis M, Varghese R, Hosseinian L, Vida V, Tarzia V, et al. Results with Syncardia total artificial heart beyond 1 year. ASAIO J. 2014;60:626–34.
11. Liska J, Lundbäck S, Semb BKH. In vitro flow characteristics of a new pump with a high inherent sensitivity to venous return. ASAIO J. 1991;37:592–7.
12. Carlsson M, Ugander M, Mosén H, Buhre T, Arheden H. Atrioventricular plane displacement is the major contributor to left ventricular pumping in healthy adults, athletes, and patients with dilated cardiomyopathy. Am J Physiol Heart Circ Physiol. 2007;292:H1452–H9.
13. Szabó Z, Holm J, Najar A, Hellers G, Ahn HC. Early experience of implantation of a new pulsatile total artificial heart (TAH) in the pig. J Clin Exp Cardiol 2017;8:1–4.
14. Szabó Z, Holm J, Najar A, Hellers G, Pieper IL, Ahn HC. Scandinavian real heart (SRH) 11 implantation as total artificial heart (TAH)-experimental update. J Clin Exp Cardiol. 2018;9:1–4.
15. Pieper IL, Sonntag SJ, Meyns B, Hadi H, Najar A. Evaluation of the novel total artificial heart Realheart in a pilot human fitting study. Artif Organs. 2020;44:174–7.
16. Fraser KH, Taskin ME, Griffith BP, Wu ZJ. The use of computational fluid dynamics in the development of ventricular assist devices. Med Eng Phys. 2011;33:263–80.
17. Behbahani M, Behr M, Hormes M, Steinseifer U, Arora D, Coronado OM, et al. A review of computational fluid dynamics analysis of blood pumps. Eur J Appl Math. 2009;20:363–97.
18. Kobayashi M, Horvath DJ, Mielke N, Shiose A, Kuban B, Goodin M, et al. Progress on the design and development of the continuous-flow total artificial heart. Artif Organs. 2012;36:705–13.
19. Sonntag SJ, Kaufmann TAS, Büsen MR, Laumen M, Linde T, Schmitz-Rode T, et al. Simulation of a pulsatile total artificial heart: development of a partitioned fluid structure interaction model. J Fluids Struct. 2013;38:187–204. https://doi.org/10.1016/j.jfluidstructs.2012.11.011
20. Sonntag SJ, Kaufmann TAS, Büsen MR, Laumen M, Gräf F, Linde T, et al. Numerical washout study of a pulsatile total artificial heart. Int J Artif Organs. 2014;37:241–52.
21. Luraghi G, De Gaetano F, Rodriguez Matas JF, Dubini G, Costantino ML, De Castilla H, et al. A numerical investigation to evaluate the washout of blood compartments in a total artificial heart. Artif Organs. 2020;44(9):976–86. https://doi.org/10.1111/aor.13717
22. Autodesk CFD Knowledge Network. What is Autodesk CFD? 2020. Available from: https://www.autodesk.com/products/cfd/overview
23. Martinolli M, Biasetti J, Zonca S, Polverelli L, Vergara C. Extended finite element method for fluid-structure interaction in wave membrane blood pump. Int J Numer Methods Biomed Eng. 2021;37:e3467.
24. Marsden AL, Bazilevs Y, Long CC, Behr M. Recent advances in computational methodology for simulation of mechanical circulatory assist devices. WIREs Syst Biol Med. 2014;6:169–88.
25. Trip R, Kuik DJ, Westerweel J, Poelma C. An experimental study of transitional pulsatile pipe flow. Phys Fluids. 2012;24(1):014103. https://doi.org/10.1063/1.3673611
26. Brindise MC, Vlachos PP. Pulsatile pipe flow transition: flow waveform effects. Phys Fluids. 2018;30(1):015111. https://doi.org/10.1063/1.5021472
27. Fraser KH, Poelma C, Zhou B, Bazigou E, Tang M-X, Weinberg PD. Ultrasound imaging velocimetry with interleaved images for improved pulsatile arterial flow measurements: a new correction method, experimental and in vivo validation. J R Soc Interface. 2017;14:20160761.
28. Escher A, Choi Y, Callaghan F, Thamsen B, Kertzscher U, Schweiger M, et al. A valveless pulsatile pump for heart failure

with preserved ejection fraction: hemo- and fluid dynamic feasibility. Ann Biomed Eng. 2020;48:1821–36.
29. Luraghi G, Wu W, De Castilla H, Rodriguez Matas JF, Dubini G, Dubuis P, et al. Numerical approach to study the behavior of an artificial ventricle: fluid-structure interaction followed by fluid dynamics with moving boundaries. Artif Organs. 2018;42:E315–24.
30. Luraghi G, Migliavacca F, Rodriguez Matas JF. Study on the accuracy of structural and FSI heart valves simulations. Cardiovasc Eng Technol. 2018;9:723–38.
31. Stewart SFC, Paterson EG, Burgreen GW, Hariharan P, Giarra M, Reddy V, et al. Assessment of CFD performance in simulations of an idealized medical device: results of FDA's first computational interlaboratory study. Cardiovasc Eng Technol. 2012;3:139–60.
32. Autodesk CFD Knowledge Network. Autodesk CFD learning guide: moving solids. 2020. Available from: https://knowledge.autodesk.com/support/cfd/learn-explore/caas/CloudHelp/cloudhelp/2021/ENU/SimCFD-Learning/files/Reference-Material/Theoretical-Background/Governing-Equations/GUID-637724EB-02CF-4195-AF55-5F9CDD08F332-html.html?st=moving%20solids
33. Versteeg HK, Malalasekera W. An introduction to computational fluid dynamics: the finite volume method. 2nd ed. Harlow: Pearson Prentice Hall; 2007.
34. Shibeshi SS, Collins WE. The rheology of blood flow in a branched arterial system. Appl Rheol. 2005;15:398–405.
35. Chaliki HP, Hurrell DG, Nishimura RA, Reinke RA, Appleton CP. Pulmonary venous pressure: relationship to pulmonary artery, pulmonary wedge, and left atrial pressure in normal, lightly sedated dogs. Catheter Cardiovasc Interv. 2002;56:432–8.
36. Sugiura T, Freis ED. Pressure pulse in small arteries. Circ Res. 1962;11:838–42.
37. Coccarelli A, Prakash A, Nithiarasu P. A novel porous media-based approach to outflow boundary resistances of 1D arterial blood flow models. Biomech Model Mechanobiol. 2019;18:939–51.
38. Boudoulas H, Geleris P, Lewis RP, Rittgers SE. Linear relationship between electrical systole, mechanical systole, and heart rate. Chest. 1981;80:613–7.
39. Fraser KH, Zhang T, Taskin ME, Griffith BP, Wu ZJ. A quantitative comparison of mechanical blood damage parameters in rotary ventricular assist devices: shear stress, exposure time and hemolysis index. J Biomech Eng. 2012;134:e081002.
40. Yu H, Engel S, Janiga G, Thévenin D. A review of hemolysis prediction models for computational fluid dynamics. Artif Organs. 2017;41:603–21.
41. Fresiello LN, Brynedal Ignell N, Zielinski K, Meyns B, Perkins IL. Hemodynamic characterization of the Realheart® total artificial heart with a hybrid cardiovascular simulator. Artif Organs. 2021, under review.
42. Molteni A, Masri ZP, Low KW, Yousef HN, Sienz J, Fraser KH. Experimental measurement and numerical modelling of dye washout for investigation of blood residence time in ventricular assist devices. Int J Artif Organs. 2018;41:201–12.
43. Pohlmann JR, Toomasian JM, Hampton CE, Cook KE, Annich GM, Bartlett RH. The relationships between air exposure, negative pressure, and hemolysis. ASAIO J. 2009;55:469–73.
44. Hartrumpf M, Albes JM, Krempl T, Rudolph V, Wahlers T. The hemodynamic performance of standard bileaflet valves is impaired by a tilted implantation position. Eur J Cardiothorac Surg. 2003;23:283–91.
45. Thamsen B, Blümel B, Schaller J, Paschereit CO, Affeld K, Goubergrits L, et al. Numerical analysis of blood damage potential of the HeartMate II and HeartWare HVAD rotary blood pumps. Artif Organs. 2015;39:651–9.
46. Wiegmann L, Thamsen B, de Zélicourt D, Granegger M, Boës S, Schmid Daners M, et al. Fluid dynamics in the HeartMate 3: influence of the artificial pulse feature and residual cardiac pulsation. Artif Organs. 2019;43:363–76.
47. Han JJ. Aeson—the Carmat total artificial heart is approved for enrollment in the United States. Artif Organs. 2021;45(5):445–6. https://doi.org/10.1111/aor.13959
48. Khalili F, Gamage PPT, Sandler RH, Mansy HA. Adverse hemodynamic conditions associated with mechanical heart valve leaflet immobility. Bioengineering. 2018;5:74.
49. Taskin ME, Fraser KH, Zhang T, Wu C, Griffith BP, Wu ZJ. Evaluation of Eulerian and Lagrangian models for hemolysis estimation. ASAIO J. 2012;58:363–72.
50. Faghih MM, Sharp MK. Modeling and prediction of flow-induced hemolysis: a review. Biomech Model Mechanobiol. 2019;18:845–81.
51. Wu W-T, Yang F, Wu J, Aubry N, Massoudi M, Antaki JF. High fidelity computational simulation of thrombus formation in Thoratec HeartMate II continuous flow ventricular assist device. Sci Rep. 2016;6:38025.

How to cite this article: Kelly NS, McCree D, Fresiello L, Brynedal Ignell N, Cookson AN, Najar A, et al. Video-based valve motion combined with computational fluid dynamics gives stable and accurate simulations of blood flow in the Realheart total artificial heart. Artif. Organs. 2022;46:57–70. https://doi.org/10.1111/aor.14056